THE ASTROPHYSICAL JOURNAL, 545:290–300, 2000 December 10


# DISTANCE LIMITS ON THE BRIGHT X-RAY EMISSION TOWARD THE GALACTIC CENTER: EVIDENCE FOR A VERY HOT INTERSTELLAR MEDIUM IN THE GALACTIC X-RAY BULGE

R. C. ALMY AND D. MCCAMMON
Department of Physics, University of Wisconsin-Madison, 1150 University Avenue, Madison, WI 53706; almy@wisp5.physics.wisc.edu, mccammon@wisp.physics.wisc.edu

S. W. DIGEL
Raytheon STX, NASA/Goddard Space Flight Center, Code 660.2, Greenbelt, MD 20771; digel@gsfc.nasa.gov

AND

L. BRONFMAN AND J. MAY
Universidad de Chile, Departamento de Astronomia, Casilla 36-D, Santiago, Chile; leo@das.uchile.cl, jmay@das.uchile.cl
*Received 1998 July 13; accepted 2000 July 25*

## ABSTRACT

Observations of the diffuse X-ray background at energies $\sim\frac{3}{4}$ and 1.5 keV show a large region of enhanced emission around the Galactic center. The origin of this X-ray enhancement is not known, but the best candidates are the nearby Loop I superbubble and a Galactic X-ray bulge. To differentiate between these two possibilities, the distance scales to the X-ray–emitting material along the line of sight must be established. A mosaic of 13 *ROSAT* PSPC pointings in the direction of $l \sim 337°$, $b \sim 4°$ reveals X-ray shadows in the $\frac{3}{4}$ and 1.5 keV bands cast by a distant molecular cloud complex. Analysis of the shadows indicates that a large fraction (45% $\pm$ 9%) of the observed emission in this direction originates beyond the cloud complex, located at $d \sim 2$ kpc. The implied surface brightness of this distant emission source can account for $\sim$70% of the enhanced emission away from the absorption trough in the Galactic plane. This result indicates that the Loop I bubble cannot be the principal source of the enhanced X-ray emission, and suggests the existence of a bright X-ray source occupying the central region of the Galaxy, with a radial extent of $\sim$6 kpc and an X-ray luminosity of $\sim 10^{39}$ ergs s$^{-1}$. We examine some simple models of the emission region and compare them to the *ROSAT* all-sky survey. A thermal origin for the emission implies a plasma temperature of $\sim 4 \times 10^6$ K and a total thermal energy in the range of 6–9 $\times 10^{55}$ ergs.

*Subject headings:* Galaxy: structure — ISM: clouds — ISM: structure — X-rays: ISM

## 1. INTRODUCTION

The diffuse soft X-ray background in the $\frac{3}{4}$ keV band is dominated by an irregular feature, roughly 110° in diameter, the center of which is located in the direction of the Galactic center. The surface brightness of this region is $\sim$6 times that of the otherwise nearly isotropic background. Observations in the 1.5 keV band show enhanced emission in the same region, although to a lesser extent ($\sim$4 times the isotropic background). Early observations (Bunner et al. 1972) established that the brightest part of this region, the Galactic-northeastern limb, is associated with the North Polar Spur, a bright radio continuum ridge that is part of Radio Loop I (Berkhuijsen, Haslam, & Salter 1971). The X-ray emission of the North Polar Spur is attributed to thermal radiation from a hot plasma, created by one or more supernovae exploding into a windswept bubble (Iwan 1980; Egger & Aschenbach 1995 and references therein). The bubble is about 150 pc in radius and centered at a distance of 170 pc (deGeus 1992; Egger 1995). The circle fit to the observed Loop I radio ridges neatly encloses most of the $\frac{3}{4}$ keV enhancement, which also shares the broadband spectral characteristics of the North Polar Spur. Consequently, it has been tempting to attribute all of the bright X-ray emission from the interior of the loop to the Loop I bubble. The near symmetry of the central parts of the enhancement about the Galactic center, however, also has suggested the possibility that this emission comes from much farther away, representing a very large and bright "Galactic X-ray Bulge" (Garmire & Nugent 1981; Snowden et al. 1997).

The large difference in distance scales between the Loop I bubble and the X-ray bulge offers a clear distinction between them as sources for the enhancement. The presence or absence of "shadows" cast by interstellar clouds at various distances could eliminate one candidate or the other. As noted by Snowden et al. (1997), the enhancement is bisected by an absorption trough in the Galactic plane. While it may be tempting to interpret the trough as evidence against the Loop I origin, it is difficult to make an entirely convincing case. Most of the dense molecular clouds identified in this region have distances of $\sim$100–200 pc, and so are not clearly located beyond the Loop I bubble. Snowden et al. (1997) estimate that the absorbing column densities required for the absorption trough are $\sim 4 \times 10^{21}$ H cm$^{-2}$. This material may be located in the foreground or within the bubble without requiring unrealistically high densities.

The *ROSAT* PSPC instrument has now made it possible to study shadows cast by interstellar clouds against the soft X-ray background on angular scales down to a fraction of a degree. Previous shadowing studies in the region of the enhanced X-ray emission have provided some evidence of emission from beyond the Loop I bubble. Observations of a nearby molecular cloud ($d \sim 200$ pc) in the direction $l = 0\overset{\circ}{.}0$, $b = -17\overset{\circ}{.}8$ revealed a deep shadow in the $\frac{3}{4}$ keV emission: 76% of the emission originates from beyond the cloud (Garmire 1992; Burrows & Mendenhall 1993). This cloud is, however, probably within the Loop I bubble, and does not completely exclude the bubble as the dominant source of the enhanced X-ray emission in the general direction of

the Galactic center. More recently, Park et al. (1997) and Park, Finley, & Dame (1998) have reported evidence of X-ray shadowing by molecular gas beyond 2.5 kpc in the Galactic plane. Interpretation of these data is complicated because of the continuous distribution of the molecular gas along the line of sight in the plane ($|b| \leq 1°$). The low X-ray surface brightness was consistent with foreground absorption in the Galactic plane. This residual low level in the plane is about the same brightness as observed in other directions, including high Galactic latitudes, where it is due to an unknown and presumably independent component. Park (1998) also detected a deep X-ray shadow cast by an *IRAS* 100 $\mu$m cloud at relatively high latitude ($b \sim -8°$), yet within the bright X-ray enhancement ($l \sim 8°$). Although this shadow appears to provide further support for the Galactic X-ray bulge, the distance scale to the molecular cloud was not firmly determined.

To rule out the Loop I origin as a principal source for the strong enhancement in the diffuse X-ray background in the direction of the Galactic center, we would like to identify an isolated molecular cloud that is clearly located beyond the far side of the Loop I bubble as well as within the X-ray enhancement. We can then determine if the cloud shadows the excess X-ray flux. We report evidence of X-ray shadows cast by a molecular cloud complex located $\sim 2$ kpc away in the direction of the X-ray enhancement. Our analysis will concentrate on the $\frac{3}{4}$ keV emission in light of the greater magnitude of the enhancement and the stronger absorption by neutral gas at this energy.

If the enhanced X-ray emission is due to a source centered on the Galactic center, there will be important implications for the structure of the interstellar medium (ISM) in the Galaxy. We will consider some simple models for such a Galactic X-ray bulge in the second half of this paper.

## 2. DATA

A search for serendipitous observations of molecular clouds was made using the HEASARC *ROSAT* public archive and the composite Galactic CO survey of Dame et al. (1987). The *ROSAT* archive was searched for pointings covering the region where the X-ray enhancement and the CO survey overlap. To avoid the X-ray absorption trough in the Galactic plane, only pointings centered on latitudes $|b| > 3°$ were considered. We confined the search to pointings centered on longitudes $|l| > 10°$ to allow the determination of kinematic distances to clouds. To ensure adequate counting statistics, only pointings with exposure times greater than 5 ks were considered. Once the candidate pointings were selected, the CO data were inspected for emission features that (1) had radial velocities indicating near kinematic distances greater than 1 kpc and (2) lacked significant emission at kinematic distances of less than 1 kpc. The best candidate turned out to be a cloud complex, G337+4, that had been observed in both the X-rays and in CO for the purpose of an X-ray shadowing study. The region of the cloud complex was covered by a group of 13 overlapping *ROSAT* PSPC pointed observations and by 170 pointings with the 1.2 m millimeter wave telescope in Cerro Tololo, Chile.

The X-ray observations are summarized in Table 1. The contamination due to noncosmic sources, i.e., particle background, scattered solar X-rays, and long-term enhancements, were modeled and subtracted according to the methods described by Snowden et al. (1994). Software for the contamination analysis is available from the US *ROSAT* Guest Observer Facility of Goddard Space Flight Center and is described by Snowden (1994). Data taken during periods of excessive particle background or short term enhancements (auroral X-rays, excess solar contamination, etc.), as indicated by anomalous peaks in the light curve, were omitted from the analysis.

TABLE 1

LIST OF *ROSAT* PSPC OBSERVATIONS

| Observation ID | $l$ | $b$ | Exposure (ks) | Dates |
|---|---|---|---|---|
| RP900498 ..... | 336.50 | 4.25 | 3.89 | 1993 Sep 5-6 |
| RP900499 ..... | 337.35 | 4.25 | 5.49 | 1993 Sep 6 |
| RP900500 ..... | 336.50 | 5.10 | 3.03 | 1993 Sep 4–9 |
| RP900501 ..... | 335.65 | 4.25 | 5.43 | 1993 Sep 4–6 |
| RP900502 ..... | 336.50 | 3.40 | 4.85 | 1993 Sep 6–7 |
| RP900503 ..... | 335.00 | 3.00 | 4.17 | 1993 Sep 5 |
| RP900505 ..... | 338.35 | 3.00 | 4.39 | 1993 Sep 21 |
| RP900506 ..... | 335.60 | 3.60 | 4.41 | 1993 Aug 25–26 |
| RP900507 ..... | 335.60 | 2.40 | 5.10 | 1993 Sep 7–9 |
| RP900508 ..... | 334.40 | 2.40 | 4.63 | 1993 Sep 6–9 |
| RP900509 ..... | 334.40 | 3.60 | 5.10 | 1993 Sep 4–5 |
| RP900510 ..... | 337.50 | 3.00 | 3.93 | 1993 Sep 7–8 |
| RP900511 ..... | 337.50 | 3.85 | 4.03 | 1993 Sep 18–19 |

The average contribution from the noncosmic background was $\sim 4\%$ of the total observed counts in the $\frac{3}{4}$ keV band and $\sim 5\%$ in the 1.5 keV band. The individual pointings with noncosmic contamination and point sources removed were merged into large-area mosaics in the $\frac{3}{4}$ keV (R4+R5) and 1.5 keV (R6+R7) bands (Snowden et al. 1994). The different pointings have relative offsets in counting rate owing to statistical fluctuations and residual contamination. These are determined by comparing average count rates in overlapping regions of all pairs of observations. The offsets are subtracted from the individual pointings in the creation of the final mosaic. These offsets are typically small compared to the total observed counts. Seven of the pointings have offsets of $\sim -9\%$ in the $\frac{3}{4}$ keV band, indicating surface brightnesses that are low relative to the other pointings. Four pointings have offsets which are higher by $\sim 10\%$, and the remaining two are higher by 19% and 28%. It thus appears that the $\sim -9\%$ offsets are the true baseline for the mosaic. The higher offsets probably indicate residual noncosmic contamination that was not successfully removed. With the noncosmic contamination and the relative offsets subtracted, the diffuse X-ray intensity of the mosaic is consistent with the flux levels of the *ROSAT* all-sky survey data for the same region. (Snowden et al. 1995). The offsets in the 1.5 keV band are smaller in magnitude, but generally consistent with the $\frac{3}{4}$ keV offsets. The X-ray mosaic was binned in $15' \times 15'$ pixels to match the sampling of the CO data. The average uncertainty in count rate for a single bin was $\sim 9\%$ in the $\frac{3}{4}$ keV band and $\sim 8\%$ in the 1.5 keV band.

The CO data were taken using the 1.2 m millimeter-wave telescope in Cerro Tololo, Chile in 1993 April and May. At 115 GHz, the frequency of the CO $J = 1$–0 rotational transition, the telescope has a beam width of $8'.8$ FWHM. The data were taken with a velocity resolution of 0.26 km s$^{-1}$, over the range from $-51.4$ to $+15.0$ km s$^{-1}$, with an rms noise of 0.25 K per channel. In order to calculate gas column densities, the antenna temperature $T_a$ must be con-

verted to main-beam brightness temperature $T_{mb}$. The calibration of the telescope yields the relationship $T_{mb} = 1.22 \times T_a$. Spectra were obtained for 170 pointings on a 15′ grid, overlapping the area of the X-ray mosaic.

Our shadowing study also used H I data taken from the southern Galactic plane survey of Kerr et al. (1986). The data were obtained using the Parkes 60 ft. telescope, which has a beam width of 48′ at 1.4 GHz. The survey data were sampled on a Galactic grid every 30′ in longitude and every 15′ in latitude. The velocity resolution was 2.1 km s$^{-1}$, with an rms noise of 0.27 K channel$^{-1}$. Although we do not expect the neutral hydrogen to be as important as the molecular gas in determining the X-ray absorption, it will be a contributing factor. Including these data allow us to take into account the general latitudinal variation in X-ray absorption.

## 3. ANALYSIS

Examination of the CO data reveals two distinct velocity components of the molecular gas. One has a radial velocity centered on +5 km s$^{-1}$ with a spread of ±2 km s$^{-1}$. We use the southern Galactic rotation curve of Alvarez, May, & Bronfman (1990) to estimate the kinematic distance. In this velocity range there is only a far value for the kinematic distance, which would place this cloud on the far side of the Galactic center (~16 kpc). However at a latitude of ~4° a cloud at this distance would be located ~1 kpc above the plane of the Galaxy, which is unlikely for CO gas. It is more likely that the radial velocity is anomalous and the cloud is located at a distance less than 500 pc. The observed region is located just below the Lupus molecular cloud complex, which has a similar radial velocity. If they are associated, this would place the cloud at a distance of about 170 pc (Dame et al. 1987 and references therein).

The rest of the emission is produced by a complex of clouds. The bulk of this emission belongs to a component whose central velocity varies from −26 to −22 km s$^{-1}$ across the observed region, with a spread in velocity at any point of about ±2 km s$^{-1}$. Using the rotation curve of Alvarez et al. (1990), and assuming a typical random variation of velocity of ±10 km s$^{-1}$, this component has a near kinematic distance of 2.3 ± 0.9 kpc or a far kinematic distance of 13.2 ± 0.9 kpc. The far kinematic distance would imply that the cloud complex be located ~0.9 kpc above the plane of the Galaxy, again an unlikely location for CO gas. We will disregard the far distance for the purposes of this paper. It is unlikely that the source of the enhanced X-ray emission is located beyond the Galactic center. Given that the distant cloud complex appears to be the principal component that casts an X-ray shadow in the enhanced emission, our assumption of the near rather than far kinematic distance seems reasonable.

While the emission seen between −26 and −22 km s$^{-1}$ provides most of the structure seen in the CO map, there are two additional components that are observed in multiple spectra. One is centered at $l = 336.^{\circ}75$, $b = 4.^{\circ}25$ and has a velocity of −20 ± 2 km s$^{-1}$ (2.0 ± 0.9 kpc). The other is centered at ($l = 335.^{\circ}75$, $b = 3.^{\circ}5$ with a velocity of −18 ± 2 km s$^{-1}$ (1.8 ± 0.8 kpc). Together these clouds account for ~86% of the observed emission. There are also various scattered emission features that are observed only in one or two pointings. On the low-velocity side of the main complex of clouds we see ~4% of the emission between −16 and −13.5 km s$^{-1}$ (~1.6 to ~1.4 kpc). The remaining 10% of the emission lies in the range from −41 to −29 km s$^{-1}$ (~3.4 to ~2.6 kpc). Figure 1 shows longitude-velocity diagrams for the CO emission, sampled periodically in latitude.

The CO data were integrated in velocity to make maps of the CO emission in the principal distance ranges. The "near cloud" map covers the velocity range from +1.83 to +7.55 km s$^{-1}$, while the "far cloud" map covers −41.07 to −13.51 km s$^{-1}$. The $H_2$ column density of the clouds can be estimated from the integrated CO brightness temperature using a conversion factor $N(H_2)/W(CO) = 1.56 \times 10^{20}$ mol cm$^{-2}$ K km s$^{-1}$ (Hunter et al. 1997). We use this column density and the interstellar absorption cross sections of Bałucińska-Church & McCammon (1992) to calculate the optical depth of the clouds. For thermal emission from a plasma with a temperature $T = 10^{6.6}$ K, unit optical depth corresponds to an atomic hydrogen column density of $\sim 2.0 \times 10^{21}$ cm$^{-2}$ in the $\frac{3}{4}$ keV band and of $\sim 3.0 \times 10^{21}$ cm$^{-2}$ in the 1.5 keV band. We find that the near cloud material has a mean optical depth of ~1.0 and a peak optical depth of ~3.2, while the far cloud material has a mean depth of ~1.5 and a peak depth of ~3.4 in the $\frac{3}{4}$ keV band. The clouds should show sufficient variation in X-ray absorption to be suitable for the shadowing study. Figure 2 shows the CO intensities for the two clouds overlaid on the X-ray data.

The angular distribution of the 21 cm column density is more uniform than the CO, which likely causes the variation in the absorbing column density. The transmission of the neutral hydrogen varies primarily with latitude, ranging from ~11% in the $\frac{3}{4}$ keV band nearest the plane to ~26% at higher latitudes. In comparison, the transmission of the molecular material varies from essentially 100% away from the cloud complexes to a minimum of ~2%. We considered 21 cm data in two velocity ranges, based on those for the CO. Emission from −12 to +12 km s$^{-1}$ was associated with the near molecular cloud, while that from −42 to −12 km s$^{-1}$ was associated with the far cloud. As the 21 cm data only sampled every 30′ in Galactic longitude, it was necessary to interpolate between adjacent longitude strips to generate 21 cm maps that matched the CO data.

The X-ray data were fitted to a three-component model consisting of an unabsorbed foreground component, an intermediate component absorbed only by the gas in the near velocity range, and a distant component absorbed by all of the observed gas:

$$I_X = I_0 + I_1 \times e^{-\tau_{near}} + I_2 \times e^{-\tau_{all}} \quad (1)$$

where $I_X$ is the observed X-ray intensity, $I_0$ the X-ray intensity from the unabsorbed foreground component, $I_1$ the emitted X-ray intensity of the intermediate component, $I_2$ the emitted X-ray intensity of the distant component, $\tau_{near}$ the optical depth of the near cloud, and $\tau_{all}$ the combined optical depth of both clouds. All three components were assumed to be uniform across the observed region. The gas transmissions were estimated assuming a $T = 10^{6.6}$ K plasma for both the intermediate and distant components; this is a reasonable temperature both for emission from the Loop I bubble (Egger & Aschenbach 1995) and for a simple Galactic X-ray bulge emission model (Snowden et al. 1997).

A $\chi^2$ surface was generated by varying $I_1$ and $I_2$, the intermediate- and far-component intensities, as free parameters. For each pair of $I_1$ and $I_2$ values, the foreground intensity, $I_0$, was adjusted to give the correct total observed X-ray intensity over the region observed. The best-fit

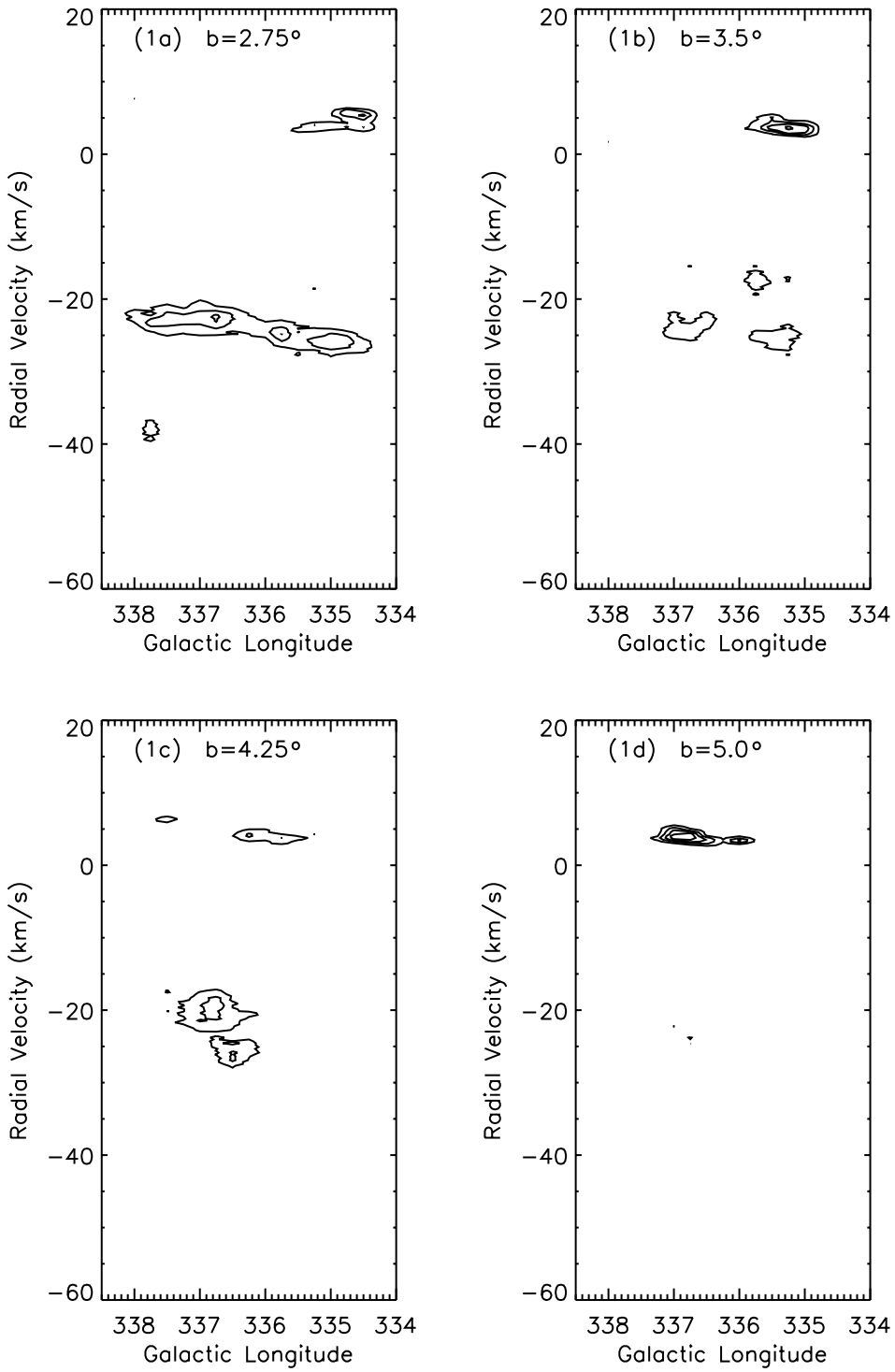


FIG. 1.—Longitude-velocity diagrams of the CO data for selected latitude cuts. Brightness temperature contours starting at 1.0 K and spaced 2.0 K. (*a*) $b = 2.^{\circ}75$. (*b*) $b = 3.^{\circ}5$. (*c*) $b = 4.^{\circ}25$. (d) $b = 5.^{\circ}0$.

models for the $\frac{3}{4}$ and 1.5 keV bands are shown in Table 2. The uncertainties reflect the range of parameters allowed at the 99% confidence level, calculated following the method outlined by Lampton, Margon, & Bowyer (1976). We see that the far component contributes approximately half of the observed emission. At this low latitude, much of the factor of $\sim 6$ enhancement has been absorbed, and the derived distant component accounts for $\sim 70\%$ of the remaining excess above the level observed in the Galactic plane away from the enhancement. The intermediate component is not statistically significant. The fit implies an upper limit on the observed emission due to the intermediate component of $28 \times 10^{-6}$ counts $s^{-1}$ arcmin$^{-1}$ in the $\frac{3}{4}$ keV band, or as much as $\sim 20\%$ of the observed emission. With the foreground emission providing $\sim 50\%$ of the emission, this still requires the distant component to provide the remaining $\sim 30\%$. In the 1.5 keV band the upper limit on the intermediate component is greater: $61 \times 10^{-6}$ counts

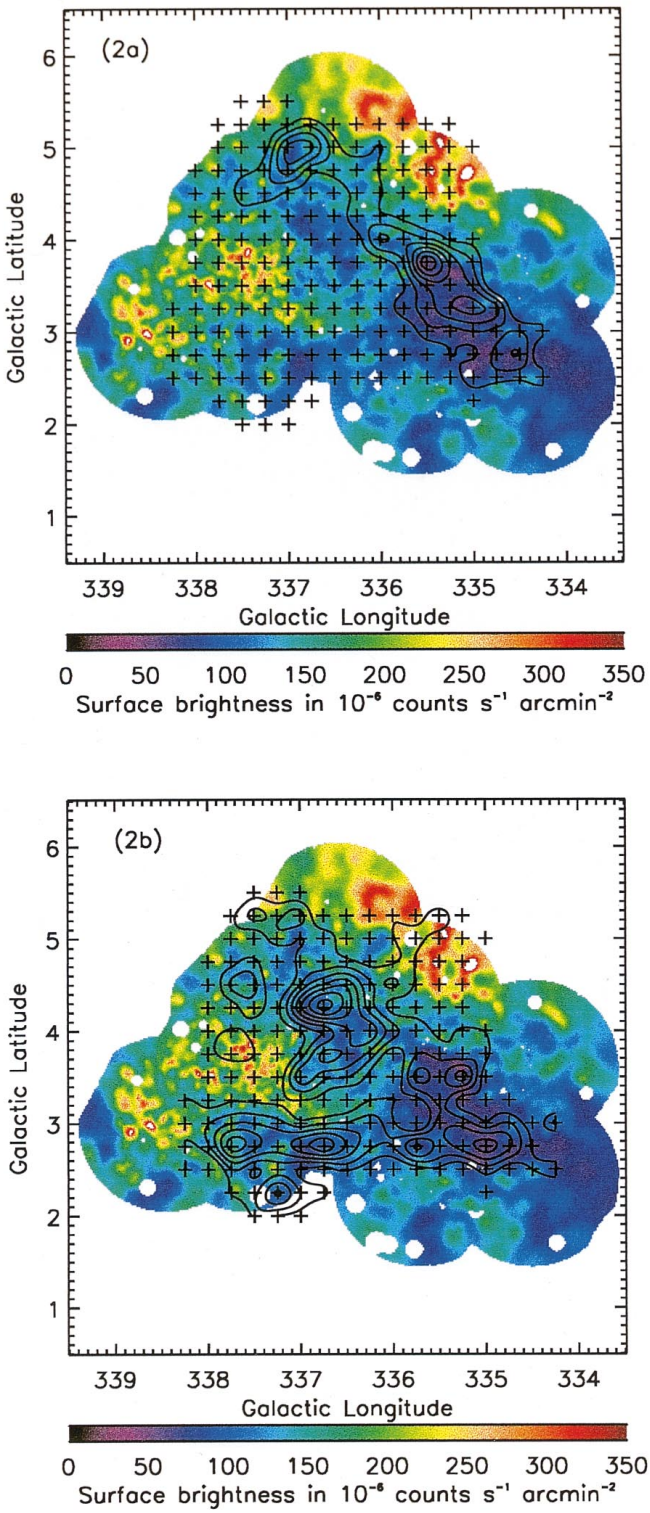


FIG. 2.—CO data (*contours*) and 3/4 keV X-ray data (*color scale*) used for the shadowing study. The X-ray data have been smoothed for display purposes only, using the adaptive smoothing algorithm described by Snowden (1994). Locations of CO observations are indicated by plus symbols. Panel (*a*) shows the CO emission from +1.83 to +7.55 km s$^{-1}$. Contours start at 3.2 K km s$^{-1}$ ($\tau \sim \frac{1}{4}$) and are spaced 3.2 K km s$^{-1}$. Panel (*b*) shows CO emission from −41.07 to −13.51 km s$^{-1}$. Contours start at 3.2 K km s$^{-1}$ and are spaced 3.2 K km s$^{-1}$.

s$^{-1}$ arcmin$^{-1}$ or ~30% of the observed emission. With the foreground component providing ~45% of the emission this still leaves a minimum contribution of ~25% from the distant component.

As the minimum values of $\chi_\nu^2$ indicate, however, the overall fit to the data is poor. This is not surprising, given the unrealistic assumption of spatially uniform emission. Figure 3 shows the observed X-ray intensity in both the $\frac{3}{4}$ keV (R45) and the 1.5 keV (R67) bands versus the total absorbing column density due to both the near and distant material. The overlaid curve shows the variation of the modeled far-component intensity as a function of column density with the modeled contribution of the near component and the average modeled contribution of the intermediate component added. The scatter plot shows a general anticorrelation between the column density and the X-ray intensity in qualitative agreement with that of the modeled distant component. This lends plausibility to the conclusion that the distant molecular cloud is shadowing a more distant emission source.

To further verify the reality of the absorption as suggested by the overall fits, we examined cuts across the observed region at constant latitude and compared the

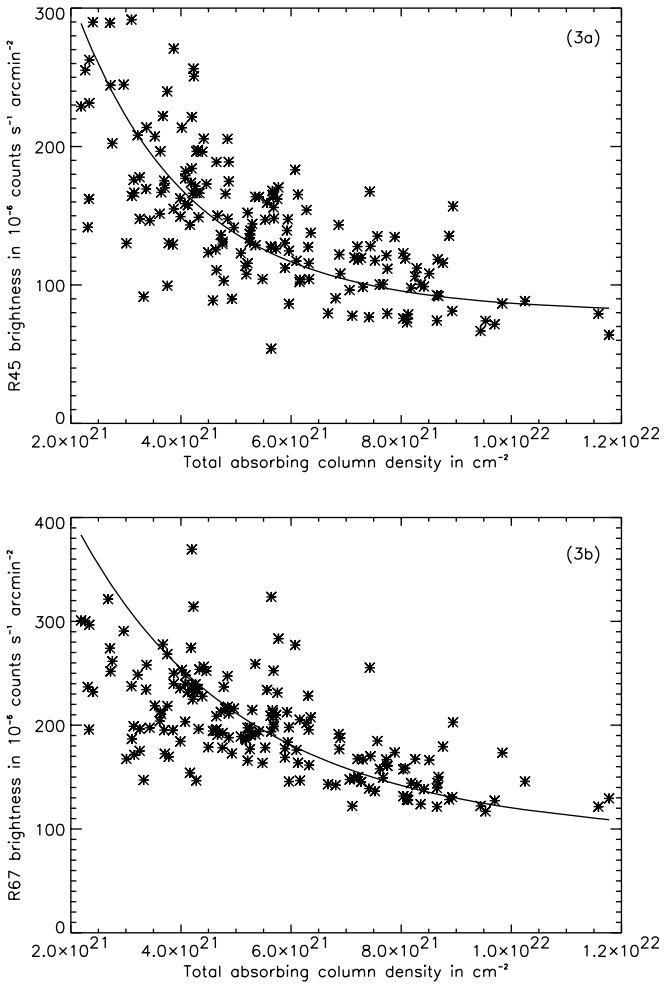


FIG. 3.—(*a*) Scatter plot of observed X-ray intensity in $\frac{3}{4}$ keV band vs. total absorbing column density. The curve shows far-component X-ray intensity as a function of column density plus the contribution for the uniform foreground component and the average contribution for the intermediate component for the best-fit three-component model. (*b*) The same except for the 1.5 keV band.

TABLE 2

THREE-COMPONENT EMISSION MODEL RESULT.

| BAND | X-RAY EMISSION ($10^{-6}$ counts $s^{-1}$ $arcmin^{-2}$) $I_0$ = Near | $I_1$ = Middle[a] | $I_2$ = Far[a] | $\nu$ | MIN. $\chi^2_\nu$ |
|---|---|---|---|---|---|
| $\frac{3}{4}$ ..... | $70 \pm 14$ | $<76$ ( $< 28$)[b] | $630 \pm 120$ (66) | 168 | 5.09 |
| 1.5..... | $89 \pm 21$ | $63 \pm 58$ (32) | $370 \pm 100$ (78) | 168 | 4.17 |

[a] Unabsorbed (average absorbed).

[b] Upper limit at 99% confidence level. The best fit value of the parameter was $26 \times 10^{-6}$ counts $s^{-1}$ $arcmin^{-2}$, for an average absorbed contribution of $9.6 \times 10^{-6}$ counts $s^{-1}$ $arcmin^{-2}$.

observed X-ray intensity to the best-fit three-component model. We considered two cuts: one comprising the observations between $b = 3.^\circ25$ *and* $3.^\circ75$, and the other covering $b = 4.^\circ0$ *to* $4.^\circ5$. These cuts include substantial variations in the column density of the far cloud and are far enough above the Galactic plane absorption trough to have an average X-ray surface brightness considerably higher than is observed in parts of the sky away from the Galactic center enhancement. The binned X-ray data and calculated gas transmissions were averaged over the latitude range for each cut at each longitude. Figure 4 shows the average values of the X-ray data along these strips, and the contributions of the various components of the best-fit three-component model. It also shows the best-fit result of a two-component model, where the near and intermediate components contribute to the emission and the far component is set to zero. The error bars on the X-ray data are statistical only. Those for the models are due to uncertainty in the gas transmission determined from the CO measurements. The good agreement of the variations with longitude for the three-component model and the difficulty in reproducing the gross variations without a substantial distant component lend further confidence to the conclusion that much of the emission lies beyond the far clouds.

## 4. DISCUSSION AND MODEL

The shadowing of the X-ray background by the cloud complex G337+4 shows that a large part of the $\frac{3}{4}$ and 1.5 keV central enhancement in this direction originates from behind 2 kpc, which is clearly beyond the Loop I superbubble. The region of the sky where G337+4 is located does not appear to be unusual. Although there may be contributions from the Loop I bubble and the unknown foreground component that provides the emission seen deep in the Galactic plane, it is likely that for the central part of the enhancement the excess beyond the isotropic background is primarily of distant origin. The most likely source for the emission beyond the Loop I bubble is the central region of the Galaxy, i.e. a Galactic X-ray bulge.

The luminosity of the X-ray bulge can be estimated independently of the emission mechanism. The observed count rate in the 0.5–2.0 keV range ($\sim 600 \times 10^{-6}$ counts $s^{-1}$ $arcmin^{-2}$) and angular size ($\sim 30^\circ$ radius) of the enhancement from the *ROSAT* all-sky survey in conjunction with the effective area of the *ROSAT* XRT/PSPC ($\sim 100$ $cm^2$) (Snowden et al. 1997) yield an estimate of the flux from the region. With a distance of 8.5 kpc to the Galactic center we estimate the luminosity in this energy range to be $\sim 10^{39}$ ergs $s^{-1}$.

Snowden et al. (1997) consider a simple single-temperature model of the enhancement and find that a plasma with normal abundances in collisional equilibrium at $\sim 4 \times 10^6$ K fits the coarse spectral characteristics of the enhancement. At this temperature the 0.5–2.0 keV luminosity is $\sim 70\%$ of the total bolometric luminosity. The thermal emission could be truly diffuse, it could be due to unresolved point sources, or it may be some combination of the two. We will investigate both diffuse and point source models of the bulge.

The simple model of Snowden et al. (1997) considers a diffuse isothermal plasma with a density that falls off exponentially with height above the Galactic plane, but is independent of radius. The plasma fills a cylinder with a radius of 5.6 kpc centered on the Galactic center. At a plasma temperature of $\sim 4 \times 10^6$ K, the model results in an electron density of 0.0035 $cm^{-3}$ at $z = 0$, a scale height of 1.9 kpc, and a pressure in the plane of $P/k_B = 2.8 \times 10^4$ $cm^{-3}$ K. The total mass is $\sim 3.3 \times 10^7$ $M_\odot$ and the thermal energy $\sim 6.4 \times 10^{55}$ ergs. The 0.5–2.0 keV X-ray luminosity is $1.9 \times 10^{39}$ ergs $s^{-1}$, in good agreement with our simple estimate above. The total luminosity is $2.8 \times 10^{39}$ ergs $s^{-1}$, implying a radiative cooling timescale of $\sim 7 \times 10^8$ yr.

This model was only intended to yield the latitude dependence near $l = 0^\circ$. It overestimates the brightness away from the center, and does not take into account known contributions from other sources. We therefore consider a more detailed model. The diffuse part is a hydrostatic model of the Galactic X-ray bulge emission developed by Wang (1997). We used a simple representation of the gravitational potential of the Galaxy (Wolfire et al. 1995), and filled it with a nonrotating plasma, which is supported against gravitational collapse by its own pressure. We assume that the plasma is described by an adiabatic polytrope, i.e., the pressure and density are related by the expression $P = k\rho^{5/3}$. These assumptions are sufficient to calculate the pressure, density and temperature of the plasma at any location in the Galaxy with only two parameters: the base pressure at the Galactic center $P_0$, and the polytrope coefficient $k$. These will be adjusted to give the observed average luminosity and spatial distribution. The resulting temperature and pressure distributions are then checked for consistency with observations.

Outside of the central enhancement, the sky in the $\frac{3}{4}$ keV band is nearly isotropic with a surface brightness of $\sim 130 \times 10^{-6}$ counts $s^{-1}$ $arcmin^{-2}$. The sources of this radiation are not all known, but we include the known components in our model of the enhancement. We have included the contributions of extragalactic point sources as described by Hasinger et al. (1993) and of normal stars using the model of Schmitt & Snowden (1990). At high

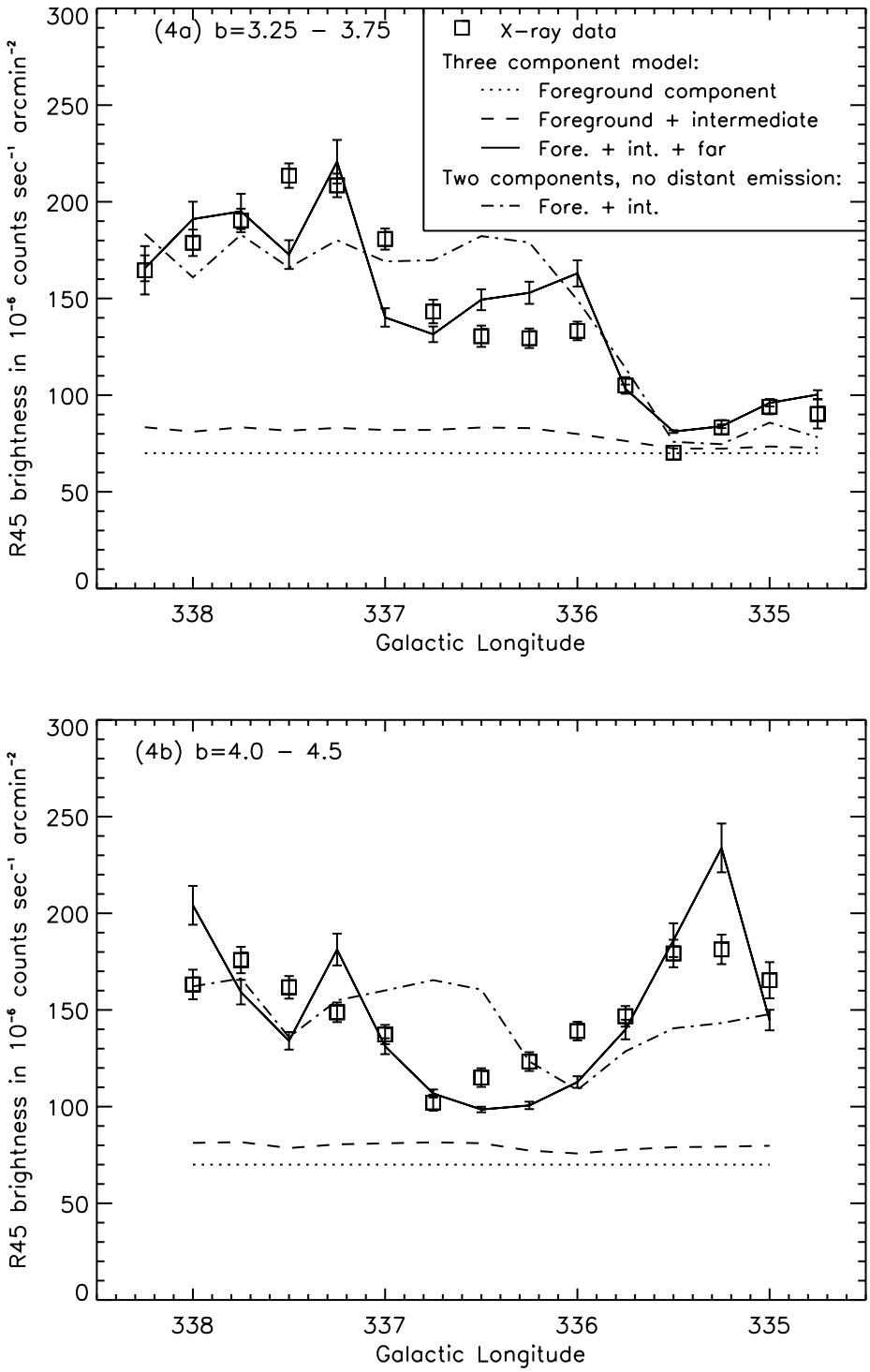


FIG. 4.—(*a*) Variation with Galactic longitude of X-ray data and the three-component model for the latitude cut from $b = 3\overset{\circ}{.}25$ to $b = 3\overset{\circ}{.}75$. The best-fit result for a model with no distant emission is shown by the dot-dash line. (*b*) The same, except for the latitude cut from $b = 4\overset{\circ}{.}0$ to $b = 4\overset{\circ}{.}5$.

Galactic latitudes, the contribution of resolved extragalactic point sources is $\sim 52 \times 10^{-6}$ counts $s^{-1}$ arcmin$^{-2}$. The stellar contribution is $\sim 9 \times 10^{-6}$ counts $s^{-1}$ arcmin$^{-2}$ at high latitudes, and peaks at $\sim 150 \times 10^{-6}$ counts $s^{-1}$ arcmin$^{-2}$ near the Galactic center and $\sim 20 \times 10^{-6}$ counts $s^{-1}$ arcmin$^{-2}$ near the anticenter. Since the extragalactic and stellar contributions do not account for all of the isotropic background, a uniform unabsorbed emission component was included in the model as a variable parameter.

The X-ray emission of the plasma was calculated using the thermal equilibrium spectral models of Raymond & Smith (1977; Raymond 1992). The absorption due to interstellar gas was estimated using the neutral hydrogen column density data of Dickey & Lockman (1990). The model was fitted to the $\frac{3}{4}$ keV band *ROSAT* all-sky survey data (Snowden et al. 1995). To avoid confusion from Loop I emission, the comparison was confined to the southern Galactic hemisphere. The sky survey data were available in

480 × 240 pixel Aitoff projection maps. We selected for our fit a 180 × 70 pixel region centered on the Galactic center in longitude and extending south from the Galactic equator in latitude. This region includes the area of the enhanced emission as well as some of the surrounding isotropic background. Data north of $b = -10°$ were initially omitted because of the uncertainty in the absorbing column density close to the plane.Extending the fit to $b = 0°$ does not significantly alter the best-fit parameters, but makes the reduced $\chi^2$ considerably worse. The emission from the hydrostatic plasma was fitted to the residual of the $\frac{3}{4}$ keV sky survey data with the extragalactic and stellar components subtracted. The parameters $k$ and $P_0$ were varied to produce a $\chi^2$ surface. The magnitude of the uniform emission component was set to provide the correct total observed count rate, averaged over the region of fit, for each combination of $k$ and $P_0$. The resulting temperature distribution was not considered at this point in the fit, but was checked for consistency with other bands as described below.

The $\frac{3}{4}$ keV data are best fitted by a central pressure of $P_0/k_B = 1.8 \times 10^5 \mathrm{cm}^{-3}$ K and a polytrope coefficient $k = 1.45 \times 10^{32}$ cm$^4$ g$^{-2/3}$ s$^{-2}$, which corresponds to a central temperature of $8.2 \times 10^6$ K and an electron density of $1.1 \times 10^{-2}$ cm$^{-3}$. The additional isotropic component for this model has a surface brightness of $59 \times 10^{-6}$ counts s$^{-1}$ arcmin$^{-2}$. Figure 5 shows the temperature, pressure and electron density of the plasma as a function of the in-plane distance from the Galactic center, $r$, and of the height above the Galactic plane, $z$. The sharp peaks in temperature and pressure at the Galactic center would flatten out in a more realistic model that included thermal conduction and energy transport; there would, however, be little change at radii greater than ~1 kpc (D. P. Cox 1998, private communication).

In the solar neighborhood the density and temperature have dropped to $\sim 8.4 \times 10^{-4}$ cm$^{-3}$ and $\sim 1.5 \times 10^6$ K, and the thermal pressure to $\sim 2.5 \times 10^3$ cm$^{-3}$ K. This is consistent with the range of pressures, $10^3$–$10^4$ cm$^{-3}$ K, observed in the Galactic disk by Jenkins, Jura, & Loewenstein (1983) using excitation of the C I fine structure levels. It is also consistent with the pressures of highly ionized halo gas, 2200 to 3700 cm$^{-3}$ K, inferred from observations of C IV emission and absorption lines by Shull & Slavin (1994). It is significantly less than the $\sim 10^4$ cm$^{-3}$ K thermal pressure in the Local Hot Bubble, which surrounds the Sun (Snowden et al. 1990).

Figure 6 compares the measured X-ray intensity and the model as a function of latitude across the region of the enhancement. We examined a subset of the region of fit containing the majority of the enhancement: the data and model components were averaged over longitudes $|l| \leq 30°$. Over most of the latitude range, the model qualitatively matches the data, although it overestimates it slightly. The region that was fitted for this model, however, does extend to greater longitudes than those included in the figure, and the model tends to underestimate the emission there. This indicates that the adiabatic polytrope probably does not have quite the right shape to fit the radial profile of the enhancement.

In Figure 7 the contributions of the polytrope, normal stars, extragalactic point sources and the isotropic component were subtracted from the $\frac{3}{4}$ keV all-sky survey data (Snowden et al. 1995). We see that in the northern Galactic

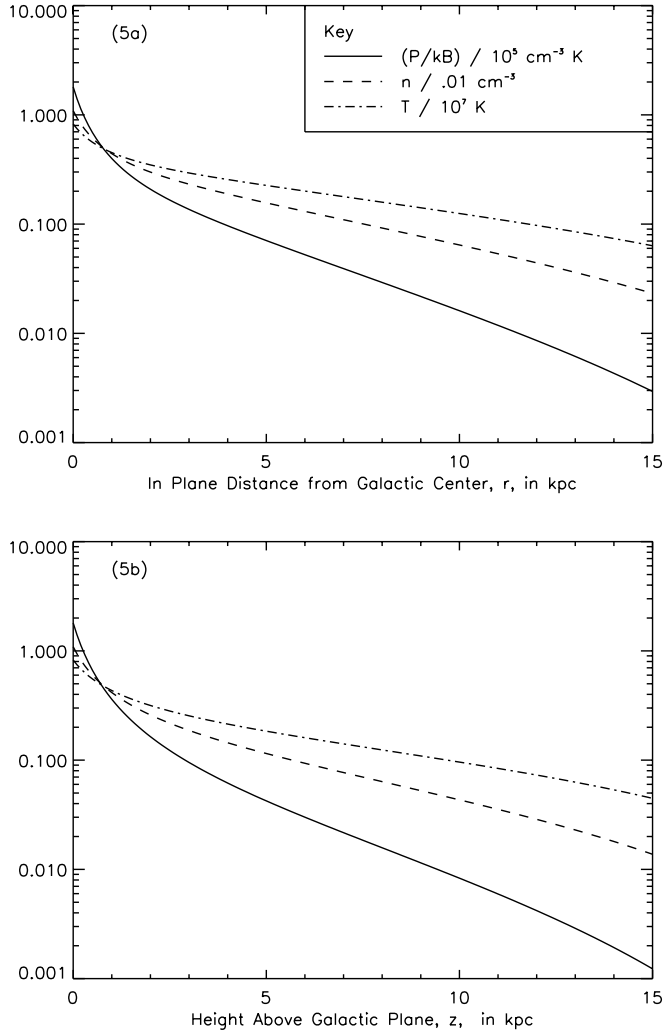


FIG. 5.—(*a*) Physical properties of the best-fit plasma in the Galactic plane ($z = 0$) as a function of distance from Galactic center, $r$. The solid line shows pressure over $k_B$ in units of $10^5$ cm$^{-3}$ K. The dashed line shows electron density in units of $10^{-2}$ cm$^{-3}$. The dot-dash line shows temperature in units of $10^7$ K. (*b*) The same, except showing variations with $z$ for $r = 0$.

hemisphere, most of the emission features within Loop I remain, and perhaps are mostly due to emission from the Loop I bubble. In the southern hemisphere, while the residual features near the bulge appear large in magnitude, they are generally only a fraction of the polytrope emission and may simply be due to inaccuracies in the absorption corrections.

We then used the best-fit parameters for the $\frac{3}{4}$ keV data to calculate the emission in the 1.5 keV band. The behavior of the model in the 1.5 keV band is similar to that in the $\frac{3}{4}$ keV band. It accounts for most of the southern hemisphere enhancement, and only partly accounts for the northern hemisphere. It overestimates the emission in the same areas as in the $\frac{3}{4}$ keV band, although less severely. Away from the central enhancement, the contribution of the model is negligible. Figure 6*b* shows the comparison of the data to the model in the 1.5 keV band. The additional isotropic component of $39 \times 10^6$ counts s$^{-1}$ arcmin$^{-2}$ was set to provide the correct surface brightness at high latitudes ($|b| > 80°$). While the central enhancement drops off more quickly with latitude in the model than in the data, the agreement

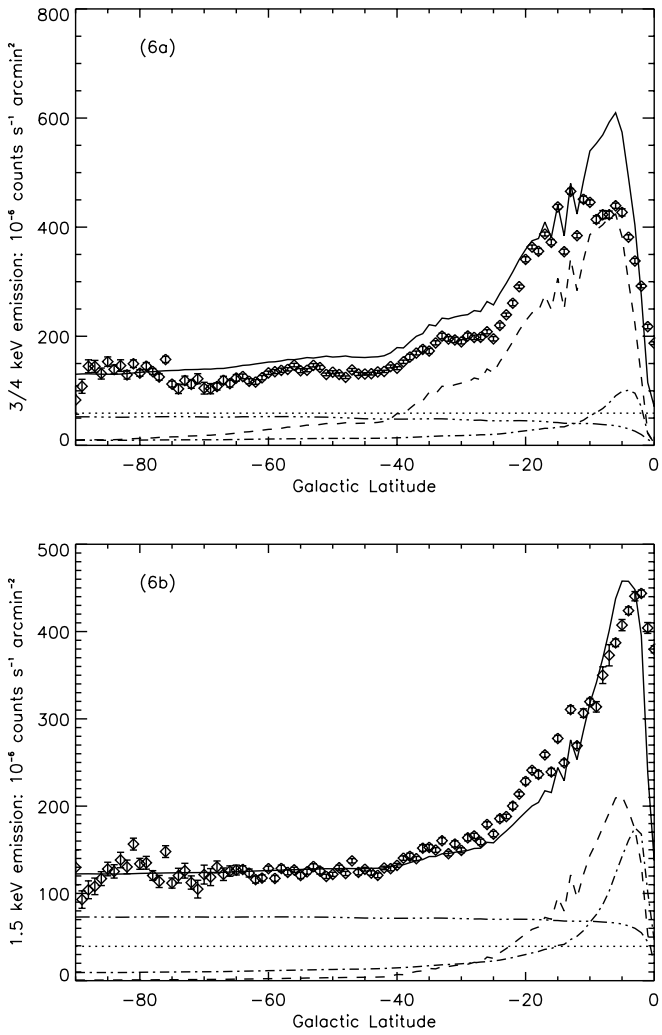


FIG. 6.—(*a*) Emission in the $\frac{3}{4}$ keV band (R4 + R5) averaged over longitudes $|l| \leq 30°$ in 1° high-latitude strips. Diamonds show the data from the *ROSAT* all sky survey (Snowden et al. 1995). The solid line shows the total modeled emission, comprising the following four components: polytrope emission (*dashed line*), emission from normal stars (*dash-dotted* line), emission from resolved extragalactic sources (*dash-dot-dot-dot line*), and the additional isotropic unabsorbed component (*dotted line*). (*b*) The same except showing the emission in the 1.5 keV band (R6 + R7).

between the two is quite close, considering that there were no free parameters in the 1.5 keV polytrope model.

Up to this point we have only shown that the model can reproduce the observed surface brightness, and have not compared the predicted temperature distribution, which is now fixed by the polytrope parameters, with the observed spectrum. Figure 8 shows the ratio of the 1.5 keV (R6 + R7) intensity to the $\frac{3}{4}$ keV (R4 + R5) intensity. The data and model were averaged over longitudes $|l| \leq 30°$. The solid line shows this hardness ratio for the full model, i.e., the polytrope, normal stars, extragalactic sources, and the unabsorbed isotropic component. The model is seen to be softer than the observed emission. For $b < -40°$ the polytrope contribution is of decreasing importance, and reasonable agreement between the observed and modeled ratios could be achieved by reducing the magnitude of the unabsorbed isotropic component in the $\frac{3}{4}$ keV band. This component has been driven up by the presence of the bright ridge seen in Figure 7 at $l \sim 325°$, which does not lie within the longitude range used for Figure 8. Removing this anomalous region from the fit would reduce the isotropic component and give good fits to both the intensity and the color at high latitudes. However, the polytrope is still somewhat too cool in the outer parts of the latitude range where the polytrope dominates ($-20°$ to $-40°$).

We also used the best-fit parameters to calculate the emission in the *ROSAT* $\frac{1}{4}$ keV (R1 + 2) band. It is important to verify that our model is not incompatible with the observations in this band. The polytrope only accounts for a small fraction of the observed intensity. In regions where the absorbing column density is low, the polytrope may produce $\sim 30\%$ of the observed intensity, but subtraction of the polytrope contribution does not significantly change the morphology of the $\frac{1}{4}$ keV emission. This is consistent with a predominantly local origin for the $\frac{1}{4}$ keV emission, as described by Snowden et al. (1990, 1998). However, it should be kept in mind that high-latitude shadowing studies (e.g., Burrows & Mendenhall 1991 and Snowden et al. 1991 ) indicate a significant contribution to the $\frac{1}{4}$ keV emission from nonlocal sources in some directions. Resolving a model of the Galactic X-ray bulge emission with the $\frac{1}{4}$ keV sky will not necessarily be a trivial matter.

Although in calculating our model we extended the polytrope plasma to large distances from the Galactic center, the volume of the plasma with temperatures below $10^6$ K does not contribute significantly to X-ray luminosity. We shall only consider the X-ray luminous volume of the polytrope plasma. For temperatures greater than $10^6$ K, the integrated mass, thermal energy, and bolometric luminosity are $\sim 1.3 \times 10^8\ M_\odot$, $\sim 8.9 \times 10^{55}$ ergs, and $\sim 8.9 \times 10^{39}$ ergs $s^{-1}$ respectively. The implied radiative cooling time scale is $\sim 3 \times 10^8$ yr. The X-ray luminosity in the 0.5–2.0 keV range is $\sim 1.2 \times 10^{39}$ erg $s^{-1}$. The remaining emission occurs at lower energies.

The portion of the polytrope at $T > 10^6$ K fills a flattened, roughly spheroidal volume with an in plane radius of $\sim 12$ kpc and a height of $\sim 10$ kpc. Snowden & Pietsch (1995) studying the face-on galaxy M101 find enhanced X-ray emission in the 0.5–2.0 keV range within a 7.5 radius of the center. With a distance of 7.2 Mpc to M101, this corresponds to a radius of $\sim 16$ kpc. They find an integrated luminosity of $3.6 \times 10^{39}$ ergs $s^{-1}$ in the 0.5–2.0 keV range, in reasonable agreement with our result. This luminosity, however, was calculated from emission at a single temperature. We compared the predictions of the polytrope model to the radial profiles of M101 and four other face-on galaxies from *ROSAT* observations reported by Cui (1994). The central pressures required to fit the profiles in the $\frac{3}{4}$ keV band were less than the value we found for our Galaxy, ranging from $P/k_B = 6.0 \times 10^4 \mathrm{cm}^{-3}$ K to $1.1 \times 10^5\ \mathrm{cm}^{-3}$ K, while the central temperatures were slightly higher, ranging from $8.4 \times 10^6$ K to $9.8 \times 10^6$ K. However, the model tended to underestimate the 1.5 keV surface brightness. We also included an estimate of the stellar contribution to the surface brightness, based on results for our own Galaxy. While this resulted in improved agreement of the model with the 1.5 keV data, the model still tended to underestimate the emission slightly, away from the centers of the galaxies. The fact that we find temperatures and pressures for these galaxies similar to our own shows that a hydrostatically supported plasma can plausibly explain X-ray bulge emission observed in other galaxies. Considering that the models employ the gravitational potential and

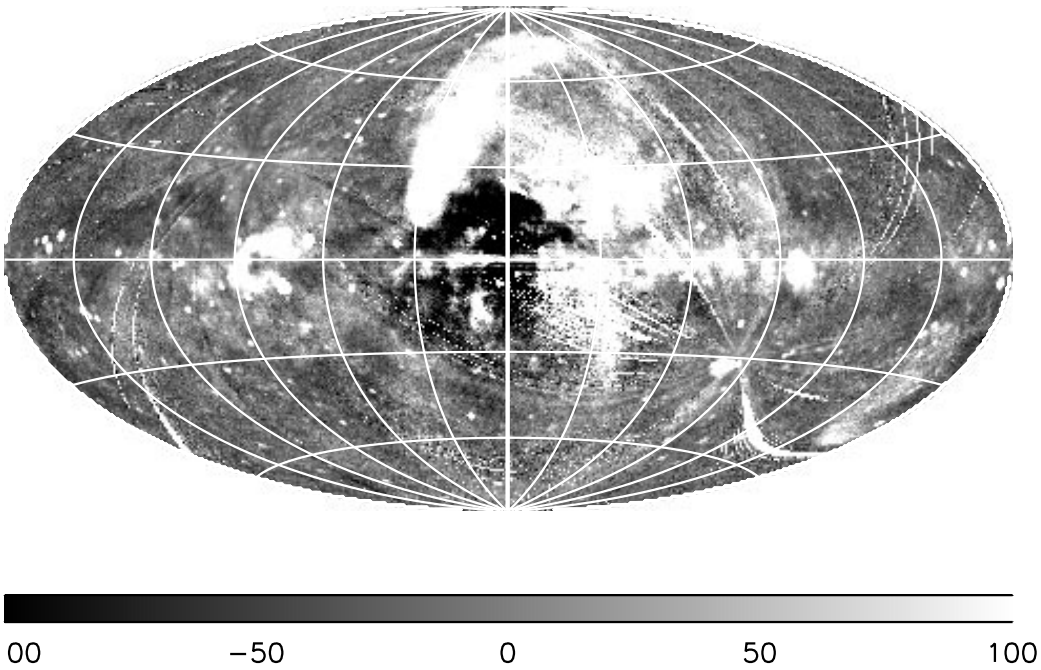


FIG. 7.—Aitoff-Hammer map of residual $\frac{3}{4}$ keV emission. The map shows the *ROSAT* all sky survey data in the $\frac{3}{4}$ keV band (Snowden et al. 1995) with the modeled emission from the polytrope, normal stars, extragalactic point sources, and the additional isotropic unabsorbed component subtracted off. The projection is an Aitoff-Hammer equal area centered on the Galactic center. The values by the scale bar show the intensity in units of $10^6$ counts $s^{-1}$ arcmin$^{-2}$.

stellar distribution of our own Galaxy, no stronger claim can be made.

The X-ray–emitting region in our polytrope model extends past the solar circle, but only a smaller central region contributes strongly to the total intensity. From its angular size, we estimate a radius of 5.6 kpc for the region producing the enhancement. At this radius, the polytrope temperature is $\sim 2.1 \times 10^6$ K. The height of the bulge at this temperature is $\sim 4.1$ kpc, which agrees with the angular size of the enhancement perpendicular to the plane. Integrating over gas with this temperature or higher, we get a total mass, thermal energy, and luminosity of $\sim 2.7 \times 10^7$ $M_\odot$, $\sim 3.0 \times 10^{55}$ ergs, and $\sim 2.4 \times 10^{39}$ ergs $s^{-1}$. These results are similar to those found for the simple model of Snowden et al. (1997): $\sim 3.3 \times 10^7$ $M_\odot$, $\sim 6.4 \times 10^{55}$ ergs, and $\sim 2.8 \times 10^{39}$ ergs $s^{-1}$, respectively. The X-ray luminosity the polytrope model in the 0.5–2.0 keV range is $\sim 8.4 \times 10^{38}$ ergs $s^{-1}$, or 70% of the X-ray luminosity for the entire plasma. This still agrees reasonably well with our simple estimate of $\sim 10^{39}$ ergs $s^{-1}$ for the X-ray luminosity based on the observed X-ray intensity from the region and Snowden et al.'s result of $1.9 \times 10^{39}$ ergs $s^{-1}$.

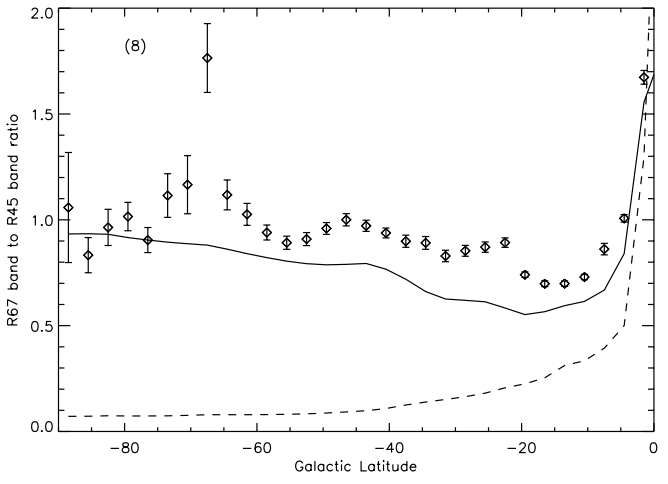


FIG. 8.—Ratio of the 1.5 keV (R6+R7) emission to the $\frac{3}{4}$ keV (R4+R5) emission. The data have been averaged over longitudes $|l| \leq 30°$ in 3° high latitude strips. The diamonds show the ratio calculated from the *ROSAT* all sky survey data (Snowden et al. 1995). The solid line shows the ratio from the full model, which comprises the polytrope emission, the contributions from normal stars and extragalactic point sources, and the additional unabsorbed isotropic component. The dashed line shows the ratio of the 1.5 keV to $\frac{3}{4}$ keV emission of the polytrope only.

A question we should consider is whether there is sufficient energy input from the Galaxy to maintain the polytrope. Observations of the X-ray emission from the Galactic Ridge indicate that the plane of the Galaxy is filled with a hot ($T = 6$–$12 \times 10^7$ K) plasma (Koyama et al. 1986b). Koyama, Ikeuchi, & Tomisaka (1986a) find that if this plasma is unconfined, a supernova rate of one every 10 yr, with $10^{51}$ ergs per SN, is required to maintain the Galactic ridge plasma. This is an energy input of $\sim 3 \times 10^{42}$ ergs $s^{-1}$; only $\sim 0.3\%$ of this energy would be required to balance the total bolometric luminosity of the polytrope. A more realistic SN rate of one every 30 yr provides $\sim 120$ times the energy required to maintain the polytrope.

It is also possible that the source of the enhancement is not diffuse. The X-ray emission of normal stars modeled by Schmitt & Snowden (1990) accounts for only a small fraction of the enhancement, but it may be possible to account for the enhancement with emission from active binary stars. Güdel et al. (1996) describe observations in Baade's window by OGLE (Optical Gravitational Lensing Experiment). From the light curves, they find large a number of chromospherically active binaries, and make an estimate of their total X-ray flux using the measured flux from nearby stars of the same type. To account for binary star systems with optical variations too small to be detected by OGLE, such

as BY Dra binaries or other types of binaries viewed nearly pole-on, they increase this estimate by an additional factor of 4. It then comes close to matching the observed $\frac{3}{4}$ keV intensity of the bulge. The estimate of the number of BY Dra binaries is based on populations in the solar neighborhood, which may not be an accurate guide to the Galactic bulge populations. Furthermore, it is not clear that the binary populations extend far enough out of the Galactic plane to account for the vertical extent of the X-ray enhancement. While active binaries may contribute to the enhancement, it is not clear that they can account for all the emission. Some diffuse component may still be necessary.

## 5. CONCLUSIONS

We performed an X-ray shadowing study of the molecular cloud complex G337+4, with the object of determining the distance to the large diffuse X-ray enhancement seen in the $\frac{3}{4}$ and 1.5 keV bands in the direction of the Galactic center. It appears that a large fraction of this emission ($45\% \pm 9\%$) originates beyond the cloud complex, located at $d \sim 2$ kpc, and therefore from beyond the nearby Loop I bubble. The implied surface brightness of this distant emission source can account for $\sim$ 70% of the enhanced emission away from the absorption trough in the Galactic plane. This provides a secure confirmation of the results of Park et al. (1997, 1998) and Park (1998). The most likely source for this emission is a Galactic X-ray bulge. Observations of other galaxies have suggested the existence of similar X-ray–emitting bulges.

Consideration of some simple emission models allow us to make some estimates of the energetics of the Galactic bulge. The distance to the emission region implies an X-ray luminosity in the 0.5–2.0 keV range of $\sim 10^{39}$ ergs s$^{-1}$. A probable thermal origin of the emission implies a plasma temperature of $\sim 4 \times 10^6$ K. While other properties are dependent on the details of the emission models, some simple diffuse models indicate thermal energies in the range of 6–9 $\times 10^{55}$ ergs and mean radiative cooling times of 3–7 $\times 10^8$ yr. These values represent plausible upper limits. Clumped emission and contributions from point sources will reduce the total thermal energy. There is still the possibility that the Loop I bubble contributes a portion of the enhanced emission, within the limits of our study. Finally, the nature of the foreground emission, that fills the Galactic plane absorption trough and provides $\sim$50% of the observed emission in our shadowing study, is still unknown, as is its relative importance in other parts of the enhancement. Further observations and analysis of the bulge region will help resolve these details.

The authors would like to thank Bob Benjamin, Don Cox, Wilt Sanders, and Steve Snowden for their helpful discussion and comments, and the US *ROSAT* Software Development Center for software used in the data reduction. This research has made use of data obtained through the High Energy Astrophysics Science Archive Research Center Online Service, provided by the NASA-Goddard Space Flight Center. R.C.A. and D.M. acknowledge support from NASA grant NAG 5-679. S. W. D. acknowledges support from NASA grant NAG 5-2473, *ROSAT* Guest Investigator Program. J. M. and L. B. acknowledge support from FONDECYT grant 8970017. L. B. acknowledges support by a Catedra Presidencial en Ciencias.

## REFERENCES

Alvarez, H., May, J., & Bronfman, L. 1990, ApJ, 348, 495
Bałucińska-Church, M., & McCammon, D. 1992, ApJ, 400, 699
Berkhuijsen, E. M., Haslam, C. G. T., & Salter, C. J. 1971, A&A, 14, 252
Bunner, A. N., Coleman, P. L., Kraushaar, W. L., & McCammon, D. 1972, ApJ, 172, L67
Burrows, D. N., & Mendenhall, J. A. 1991, Nature, 351, 629
———. 1993, in AIP Conf. Proc. 313, The Soft X-Ray Cosmos, ed. E. M. Schlegel & R. Petre (Woodbury: AIP), 16
Cui, W. 1994, Ph.D. thesis, Univ. Wisconsin, Madison
Dame, T. M., et al. 1987, ApJ, 322, 706
de Geus, E. J. 1992, A&A, 262, 258
Dickey, J. M., & Lockman, F. J. 1990, ARA&A, 28, 215
Egger, R. J. 1995, in ASP Conf. Ser. 80, The Physics of the Interstellar Medium and the Intergalactic Medium, ed. A. Ferrara, C. Heiles, C. F. McKee, & P. Shapiro (San Francisco: ASP), 45
Egger, R. J., & Aschenbach, B. 1995, A&A, 294, L25
Garmire, G. P. 1992, BAAS, 24, 689
Garmire, G. P., & Nugent, J. J. 1981, BAAS, 13, 786
Güdel, M., Guinan, E. F., Margheim, S., & Kang, Y. W. 1996, Paul Scherrer Institute, Ann. Rep., 135
Hasinger, G., Burg, R., Giacconi, R., Hartner, G., Schmidt, M., Trümper, J., & Zamorani, G. 1993, A&A, 275, 1
Hunter, S. D., et al. 1997, ApJ, 481, 205
Iwan, D. 1980, ApJ, 239, 316
Jenkins, E. B., Jura, M., & Loewenstein, M. 1983, ApJ, 270, 88
Kerr, F. J., Bowers, P. F., Jackson, P. D., & Kerr, M. 1986, A&AS, 66, 373
Koyama, K., Ikeuchi, S., & Tomisaka, K. 1986a, PASJ, 38, 503
Koyama, K., Makishima, K., Tanaka, Y. & Tsunemi, H. 1986b, PASJ, 38, 121
Lampton, M., Margon, B., & Bowyer, S. 1976, ApJ, 208, 177
Park, S. 1998, Ph. D. thesis, Purdue Univ.
Park, S., Finley, J. P., & Dame, T. M. 1998, ApJ, 509, 203
Park, S., Finley, J. P., Snowden, S. L., & Dame, T. M. 1997, ApJ, 476, L77
Raymond, J. C. 1992, ApJ, 384, 502
Raymond, J. C., & Smith, B. W. 1977, ApJS, 35, 419
Schmitt, J. H. M. M., & Snowden, S. L. 1990, ApJ, 361, 207
Shull, J. M., & Slavin, J. D. 1994, ApJ, 427, 784
Snowden, S. L. 1994, Cookbook for Analysis Procedures for *ROSAT* XRT/PSPC Observations of Extended Sources and the Diffuse Background, HEASARC/USRSCD, GSFC
Snowden, S. L., Cox, D. P., McCammon, D., & Sanders, W. T. 1990, ApJ, 354, 211
Snowden, S. L., Egger, R., Finkbeiner, D. P., Freyberg, M. J., & Plucinsky, P. P. 1998, ApJ, 493, 715
Snowden, S. L., et al. 1997, ApJ, 485, 125
———. 1995, ApJ, 454, 643
Snowden, S. L., McCammon, D., Burrows, D. N., & Mendenhall, J. A. 1994, ApJ, 424, 714
Snowden, S. L., Mebold, U., Hirth, W., Herbstmeier, U., & Schmitt, J. H. M. M. 1991, Science, 252, 1529
Snowden, S. L., & Pietsch, W. 1995, ApJ, 452, 627
Wang, Q. D. 1997, in IAU Colloq. 166, The Local Bubble and Beyond, ed. D. Breitschwerdt, M. Freyberg, & J. Trümper (Springer: Berlin), 503
Wolfire, M. G., McKee, C. F., Hollenbach, D., & Tielens, A. G. G. M. 1995, ApJ, 453, 673